Separation and Purification Technology 309 (2023) 123108

Contents lists available at ScienceDirect

Separation and Purification Technology

journal homepage: www.elsevier.com/locate/seppur

Encapsulating covalent organic frameworks (COFs) in cellulose aerogels for efficient iodine uptake

Zhipeng Zhang, Xiansong Shi *, Xingyuan Wang, Zhe Zhang, Yong Wang *

State Key Laboratory of Materials-Oriented Chemical Engineering, College of Chemical Engineering, Nanjing Tech University, Nanjing 211816, Jiangsu, PR China

ARTICLE INFO

Keywords:
Covalent organic frameworks
Cellulose
Aerogel
Iodine uptake
Adsorption

ABSTRACT

Efficient capture and storage of radioiodine are of great importance for developing nuclear energy and tackling nuclear waste, which however remain challenging due to the scarcity of powerful materials. In this work, we rationally design and fabricate a hybrid material by encapsulating covalent organic frameworks (COFs) into ultralight cellulose aerogels for efficient iodine (I_2) capture. Two kinds of functionalized cellulose precursors that can be covalently cross-linked are synthesized. Solvothermally synthesized COF particles with a uniform diameter of ~ 500 nm are then introduced into the precursors followed by freeze drying to produce hybrid aerogels. With the presence of rich and ordered micropores afforded by COFs, these highly porous aerogels exhibit excellent organic solvent absorption performances and high uptake capacities toward solvent-dissolved and vaporized I_2. More importantly, in view of the processable and robust structure, we realize the shaping of hybrid aerogels into aerogel columns to effectively capture I_2 vapor and I_2 solute in continuous operations. Therefore, this work not only provides a new way to shape COF materials but also could inspire the design of viable platforms for high-performance I_2 capture.

1. Introduction

With the growth of global demands for energy, nuclear power has become an indispensable energy source due to low carbon footprint and high energy density. [1,2] However, the running of nuclear reactors produces gaseous radioactive substances which are highly detrimental to environment and humans.[3] In particular, radioiodine ^{129}I is considered as the most hazardous nuclear waste because of its long half-life (~1.57×10^7 years) and persistent damages to ecosystems.[4] Moreover, radioactive I_2 is highly mobile and easy to be dissolved in water, thus threatening the health of human beings and other living organisms.[5,6] Thus, efficiently tackling radioiodine dominates the development of nuclear energy, which however remains a challenging task due to the lack of powerful materials.

Covalent organic frameworks (COFs) are a class of emerging porous crystalline polymers composed of periodic skeletons and permanent porosity.[7–11] The reticular chemistry endows COFs with significant advantages, including low density, high surface area, physicochemical stability and pore functionality, which make COFs promising candidates to develop high-performance adsorbents. In the past five years, burgeoning COFs have been extensively studied as I_2 sorbents and exhibit superior performances over traditional materials such as activated carbon[12], zeolites[13], porous organic polymers (POPs)[14] and metal–organic frameworks (MOFs)[15]. As a matter of fact, imine-linked COFs inherently feature high nitrogen contents and electron-rich π-conjugated systems, thus affording prominent binding sites for adsorption.[16] Jiang and co-workers previously revealed that vertically aligned channels of two-dimensional COFs benefit for the sufficient capture of I_2 molecules.[17] These studies actively guide the screening of COF materials for high-capacity I_2 uptake. However, the hyper-crosslinking and non-dissolvable nature of frameworks results in a typical powder form of COFs, making them difficult to process and recycle.[18,19] Recently, COF-based aerogels with desirable processibility emerge as an alternative to address the above limitations.[20,21] As a kind of highly porous and ultralight materials, aerogels have been widely applied in the field of adsorption.[22] Thus, together with the long-range ordered structures and abundant adsorption sites, COF-based aerogels hold huge potentials in the removal of radioiodine.

Nano-structured celluloses including cellulose nanofibril (CNF) and cellulose nanocrystal (CNC) are able to produce light porous materials, especially aerogels, due to their high aspect ratio, high mechanical strength, renewability and biodegradability.[23,24] Particularly,

* Corresponding author.
E-mail addresses: xsshi@njtech.edu.cn (X. Shi), yongwang@njtech.edu.cn (Y. Wang).

https://doi.org/10.1016/j.seppur.2023.123108
Received 2 October 2022; Received in revised form 23 December 2022; Accepted 2 January 2023
Available online 2 January 2023

hydroxyl-enriched celluloses are capable of stabilizing organic additives through strong H-bonding interactions, which promises a stable introduction of COFs.[25] Also importantly, nanocelluloses have been found to stabilize colloidal solutions,[26] further ensuring the feasibility of encapsulating COFs in cellulose aerogels. Several efforts have been made to combine COFs with nanocelluloses. For example, the mixed-dimensional assembly of COF nanosheets and cellulose nanofibers could generate a narrowed sieving size for advanced separations.[27] Moreover, COF-nanocellulose composites prepared by introducing functionalized celluloses into the crystallization process exhibit an improved specific surface area and thermal stability.[28] In spite of these achievements, the design and synthesis of COF/cellulose hybrid aerogels remain unexplored.

In this work, we encapsulate nano-sized COF particles into functionalized celluloses followed by freeze drying to fabricate hybrid aerogels for highly efficient I_2 capture and recycling. This strategy allows uniform dispersion, tunable loadings and robust encapsulation of crystalline COF particles, leading to significant practical application potentials. The obtained hybrid aerogels display a high absorption capacity toward organic solvents and excellent uptake performances toward solvent-dissolved and vaporized I_2. In addition, we demonstrate the feasibility of dynamic I_2 capture by shaping hybrid aerogel into aerogel columns.

2. Experimental section

2.1. Materials

All chemicals and reagents were used as received. Microcrystalline cellulose (length: 25 μm), sodium carboxymethyl cellulose (CMC, 100 %), acidic cation exchange resin (99.7 %), sodium periodate (98 %), adipic acid dihydrazide (98 %), *N*-hydroxysuccinimide (97 %) and *p*-phenylenediamine (Pa, 97 %) were purchased from Aladdin. *N*′-ethyl-*N*-(3-dimethylaminopropyl)-carbodiimide (98 %) was purchased from TCI. 1,3,5-Triformylbenzene (Tb, 98 %) was provided by Jilin Chinese Academy of Sciences-Yanshen Technology. Iodine (^{127}I, 99.8 %), sulfuric acid (98 %), dimethyl sulfoxide (99 %), 1,4-dioxane (99 %), acetic acid (99.5 %), tetrahydrofuran (99 %), *n*-hexane (99 %), ethanol (99 %) and ethylene glycol (99 %) were obtained from Sinopharm Chemical Reagent. Deionized water (conductivity: 2–10 μS cm^{-1}) was used in all experiments.

2.2. Solvothermal synthesis of COF-LZU1

Tb (48 mg, 0.3 mmol) and Pa (48 mg, 0.45 mmol) were ultrasonically dissolved in 4 mL of 1,4-dioxane in a glass tube. Then, 0.6 mL of 3 mol L^{-1} acetic acid aqueous solution was added and the tube was flash frozen in a liquid nitrogen bath (77 K). After degassing by three freeze–pump–thaw cycles, the tube was flame sealed and heated at 120 °C for 3 days. The product was generated as yellow precipitates which were collected by filtration and further washed with 1,4-dioxane and tetrahydrofuran for several times. The final product was vacuum dried at 80 °C for 12 h.

2.3. Preparation of hybrid aerogels and pure cellulose aerogels

COF-cellulose hybrid aerogels were prepared by a sol–gel process. COF-LZU1 particles with assigned mass proportions were firstly suspended into a 1 wt% aldehyde-modified CNCs (CNCs-CHO) aqueous suspension by probe sonication for 30 min. Then, the resulting suspension was mixed with an equal volume of 1 wt% hydrazide-modified CMC (CMC-$NHNH_2$) aqueous suspension and continuously sonicated for 30 min. The obtained suspension was transferred into a freezer (−20 °C) and left undisturbed for 12 h. Next, aerogels were produced by freeze-drying the above ice-gel. The hybrid aerogels with 9, 20, 33 and 50 wt % COF-LZU1 loadings were prepared by adding the corresponding mass proportions of COF-LZU1 particles. Pure cellulose aerogels were prepared by directly mixing an equal volume of 1 wt% CNCs-CHO aqueous suspension and 1 wt% CMC-$NHNH_2$ aqueous suspension with the other conditions unchanged.

2.4. Characterization

Morphologies of the samples were imaged by a HITACHI S-4800 field-emission scanning electron microscopy (SEM) at an accelerating voltage of 3 kV. All samples were ion-sputtered with a thin layer of gold to enhance the conductivity before observations. Elemental analysis was conducted using energy dispersive X-ray spectroscopy (EDX, EMAX X-act) and X-ray photoelectron spectroscopy (XPS, 250xi, Thermo Fisher). Fourier transform infrared (FTIR) spectra were acquired on a Thermo Nicolet8700 spectrometer in the 4000–400 cm^{-1} range. Powder X-ray diffraction (PXRD) patterns were recorded on a Rigaku Smart Lab X-ray diffractometer using Cu Kα radiation (λ = 0.15418 nm) at a scan speed of 4° min^{-1} and a step size of 0.02 in 2θ. Aerogels were pressed into flat plates under a mechanical pressure of 10 MPa for PXRD measurements. Nitrogen sorption measurements were performed on a Micrometrics ASAP2460 surface area and porosity analyzer at 77 K. Thermal gravimetric analysis (TGA) was recorded by a thermal analyzer (NETZSCH STA449F3) in N_2 atmosphere with the temperature ranging from 25 to 800 °C and a heating rate of 10 °C min^{-1}.

3. Results and discussion

3.1. Structural insights of COF-LZU1

As illustrated in Fig. 1**a**, COF-LZU1 is synthesized by the solvothermal condensation of Tb and Pa, which shows macroscopically yellow powders and microscopically spherical particles with a diameter of ~ 500 nm (**Figure S4**). FTIR spectra show that the characteristic stretching vibrations of C═O (1695 cm^{-1}) for Tb and N—H (3204–3375 cm^{-1}) for Pa disappear upon the reaction (Fig. 1**b**). Meanwhile, a new peak of stretching vibration at 1625 cm^{-1} for C═N is observed, suggesting the formation of imine linkages.[29] The remarkable diffraction peak at 4.7° in the PXRD pattern agrees well with the simulated result, suggestive of the well-crystallized framework (Fig. 1**c**).[30] In addition, the synthesized COF-LZU1 shows a high porosity and a Brunauer-Emmett-Teller surface area of 249 m^2 g^{-1} (Fig. 1**d**). With the foregoing results, we demonstrate the synthesis of highly crystalline COF-LZU1.

3.2. Preparation and characterization of hybrid aerogels

Having confirmed the crystalline and porous feature of COF-LZU1, hybrid aerogels were then prepared by adding COF-LZU1 particles during the sol–gel process (Fig. 2). In this work, pure cellulose aerogels were synthesized by freeze-drying a suspension composing of 1 wt% CNCs-CHO and 1 wt% CMC-$NHNH_2$. The covalent crosslinking between CNCs and CMC allows the generation of mechanically stable, ultralight aerogels (**Figure S5**).[31] Note that, the rigid CNCs and flexible CMC endow the resulting aerogel with structural strength and elasticity, respectively.[32] Next, hybrid aerogels are accessible by dispersing the nanoscale COF-LZU1 particles into the suspension used for the preparation of pure cellulose aerogels. It is worth noting that the spatial crosslinking of two functionalized celluloses potentially ensures a robust encapsulation of COF-LZU1, preventing its leakage from the formed hybrid aerogel. The physical entanglement and van der Waals interactions between COF-LZU1 and celluloses additionally contribute to stabilizing the encapsulation of COF-LZU1.[27]

Fig. 3**a** shows the uniformly colored hybrid aerogel, implying a homogeneous distribution of COF-LZU1. Thanks to the only involvement of light elements, the prepared hybrid aerogel with 33 wt% COF-LZU1 affords a low density of ~ 15 mg cm^{-3}, which can be stably seated on

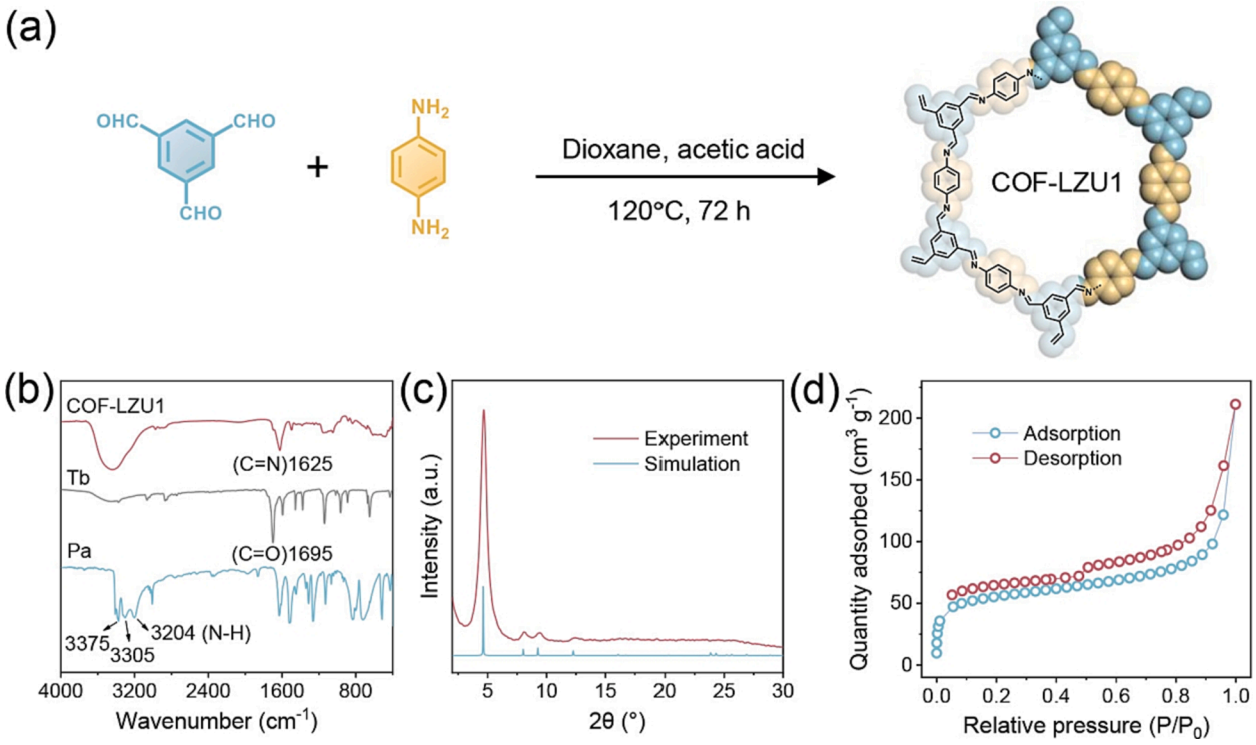

Fig. 1. Synthesis and characterization of COF-LZU1. (a) Reaction scheme of COF-LZU1. (b) FTIR spectra of Tb, Pa, and COF-LZU1. (c) Experimental and simulated PXRD patterns. (d) N_2 adsorption–desorption isotherms.

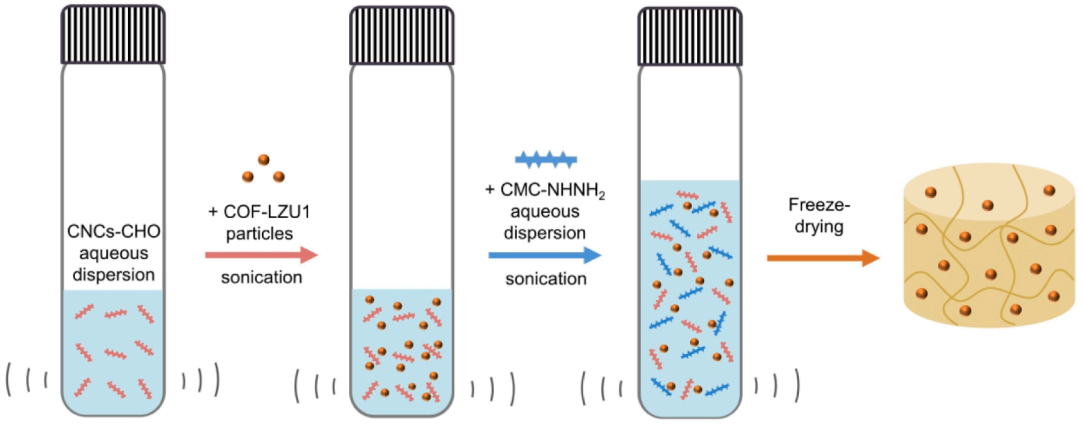

Fig. 2. Schematic diagram for the preparation of hybrid aerogels.

a dandelion. PXRD patterns reveal high crystallinity of COF-LZU1 in the hybrid aerogel (Figure S6). Moreover, the sol–gel process coupled with freeze-drying also enables the dimensional regulation of aerogels. By simply altering the size and shape of moulds, the three-dimensional structure of hybrid aerogels can be effectively regulated (Figure S7). Additionally, hybrid aerogels with the relative amounts of COF-LZU1 in the range of 9–50 wt% can be precisely fabricated (Figure S8). Particularly, as the COF-LZU1 amount reaches 50 wt%, the hybrid aerogel still keeps intact with no sign of collapse. The structural insights of these aerogels were then deeply studied by SEM imaging. At a low magnification, all the aerogels present an interlaced sheet-like morphology delivering a highly porous configuration (Figure S9). The morphologic result indicates a negligible impact of COF-LZU1 on the assembled structure of aerogels. At a high magnification, however, the structure of hybrid aerogels significantly differs from that of the neat cellulose counterpart. To be specific, nodule-structured surfaces are visibly observed for the hybrid aerogel with a low COF-LZU1 addition of 9 wt%, in sharp contrast to the smooth surface shown by the neat aerogel (Fig. 3**b** and Figure S10**a**). The nodule-structured surfaces become more significant with the increase of COF-LZU1 amounts. As the COF-LZU1 loading reaches 33 and 50 wt%, the high-magnification surfaces exhibit a rough topography largely scattered with nanoparticles (Fig. 3**c, d** and Figure S10**b, c**). These nanoparticles are in fact the introduced COF-LZU1 by considering their identical size and shape. More importantly, COF-LZU1 additives are tightly wrapped by celluloses, which effectively eliminates the loss of COF-LZU1 during practical use. In addition to the observations from above structural variations, the gradually increased loading of COF-LZU1 in hybrid aerogels is also demonstrated by the EDX mapping images. The result shows that the tagged sign of N, which exclusively originates from COF-LZU1, is

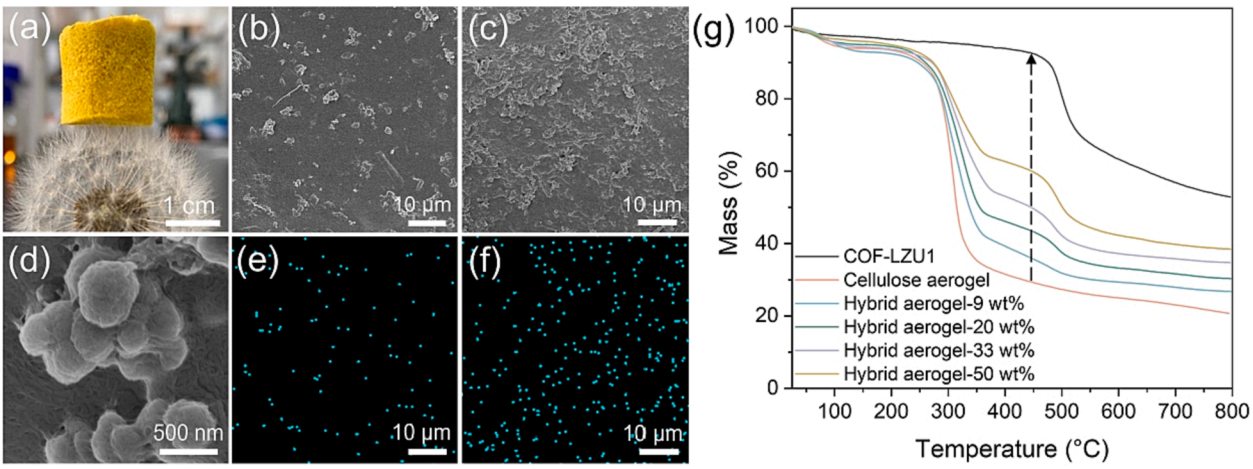

Fig. 3. Characterization of the hybrid aerogels. (a) Photograph of the hybrid aerogel with 33 wt% COF-LZU1. SEM images of the hybrid aerogels with (b) 9 wt% and (c, d) 33 wt% COF-LZU1. EDX mapping images of the hybrid aerogels with (e) 9 wt% and (f) 33 wt% COF-LZU1. (g) TGA curves of the COF-LZU1 powder, cellulose aerogel and hybrid aerogels.

increasingly intensified as the loading increases from 9 to 50 wt% (Fig. 3**e, f** and **Figure S11**). Next, we quantificationally studied the actual loading of COF-LZU1 in the prepared hybrid aerogels by TGA tests. As shown in Fig. 3**g**, upon stipulating the residual mass of the neat cellulose aerogel at 450 °C as the baseline, the residual mass of hybrid aerogels basically matches with the experimentally designated loading

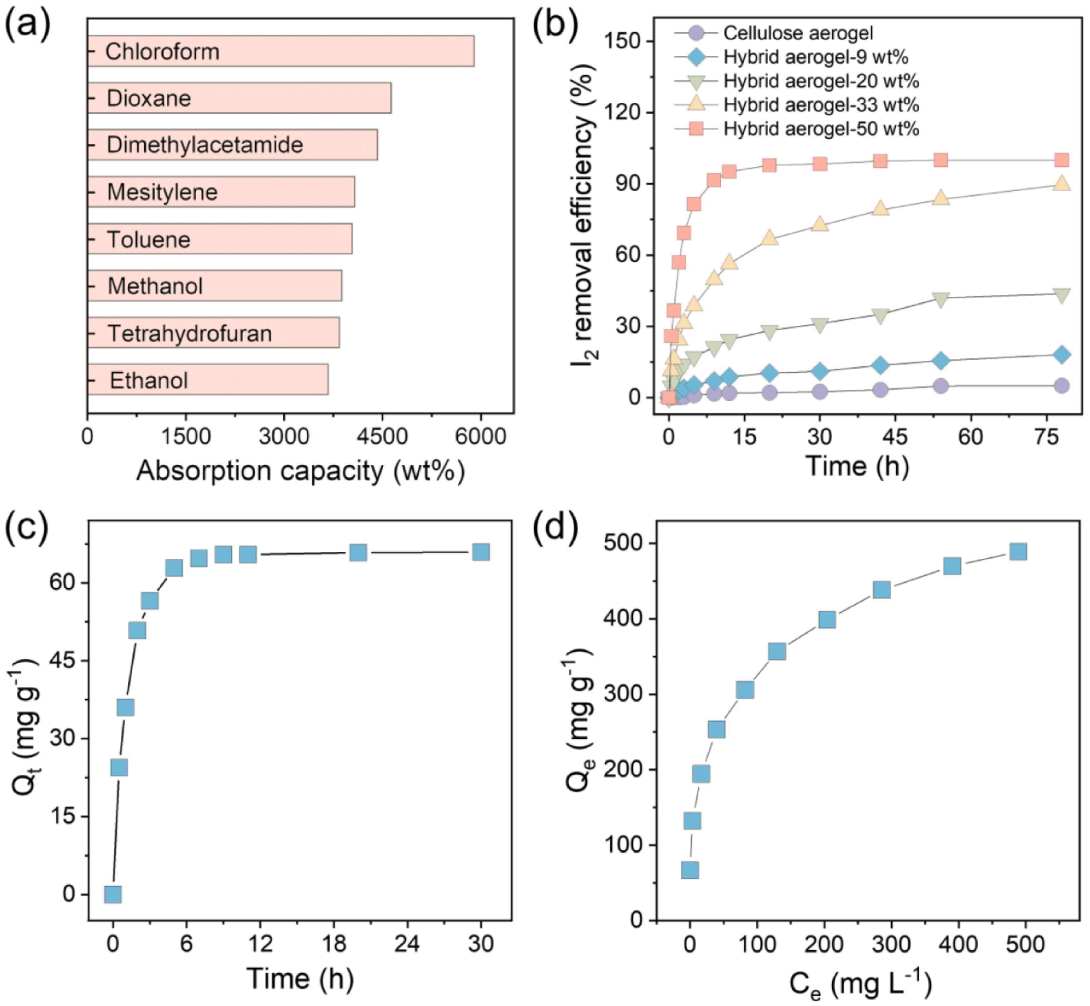

Fig. 4. Sorption ability of the fabricated pure and hybrid aerogels. (a) Solvent absorption performance of the hybrid aerogel. (b) I_2 removal efficiency of the pure cellulose and hybrid aerogels as a function of time. (c) Time-dependent I_2 uptake capacity of the hybrid aerogel. (d) Concentration-dependent I_2 uptake capacity of the hybrid aerogel.

value (Table S1). The result manifestly illustrates the consistency between the theoretic and actual mass proportion of COF-LZU1.[33]

3.3. I_2 uptake of hybrid aerogels in liquids

To elucidate a highly porous structure of hybrid aerogels, we first carried out the absorption tests towards various pure organic solvents. As shown in Fig. 4**a,** a range of common organic solvents was applied for the absorption tests. The result shows that the hybrid aerogel with 33 wt % COF-LZU1 possesses a prominent absorption capacity of approximately 36–60 times over its original weight. This excellent absorption performance indicates the rich and accessible pores of our hybrid aerogels, making them highly promising for I_2 uptake. Subsequently, we investigated the I_2 uptake performances of the pure cellulose and hybrid aerogels with different COF-LZU1 loadings in *n*-hexane solutions. The appearance change of the I_2 solutions (200 mg L^{-1}) was monitored with the soaking of aerogels. Clearly, the color of solutions involving the hybrid aerogels with 33 wt% and 50 wt% COF-LZU1 gradually fades as the duration extends, and basically colorless solutions are observed after 78 h (Figure S12). To accurately determine the removal efficiency, we tested the concentration of I_2 solutions as a function of soaking durations by UV–vis spectra. As shown in Fig. 4**b**, an efficient I_2 removal efficiency about 90 % can be achieved for the hybrid aerogels with 33 wt% and 50 wt% COF-LZU1. In contrast, the aerogels with no and low COF-LZU1 loadings yield an unsatisfactory removal efficiency, indicating the major contribution of COF-LZU1 toward I_2 uptake. After tests, the hybrid aerogel with 33 wt% COF-LZU1 keeps intact, whereas the structure of the hybrid aerogel with 50 wt% COF-LZU1 collapses. Thus, the hybrid aerogel with 33 wt% COF-LZU1 was selected for the following studies in liquids.

30 mg of hybrid aerogel with 33 wt% COF-LZU1 was used to study the uptake kinetics of I_2. The obvious change in color of I_2 *n*-hexane solution evidently confirms the viability of hybrid COF-LZU1/cellulose aerogels for high-performance I_2 capture and finally reaches an equilibrium adsorption capacity of 66.7 mg g^{-1} (Fig. 4**c** and Figure S13). The uptake result was then fitted by pseudo-first-order and pseudo-second-order models. The corresponding linear fitted curves are shown in Figure S14 and the kinetic parameters are listed in Table S2. The correlation coefficient (R^2) of the pseudo-first-order model and pseudo-second-order model is 0.601 and 0.999, respectively. Results of these indicate a pseudo-second-order uptake kinetics process in the form of chemisorption. To gain in-depth understandings on the uptake behavior of hybrid aerogels toward I_2, the adsorption isotherm was also explored. It should be noted that I_2 could not be completely adsorbed in the solutions with extremely high concentrations (Figure S15). The equilibrium uptake capacity as a function of equilibrium concentration is depicted in Fig. 4**d**. Obviously, the equilibrium adsorption capacity exhibits a positive correlation with the initial concentration of I_2 solutions. The dependency can be mainly attributed to the raise of molecular driving force with the increased initial concentration, which facilitates the penetration of I_2 into the channels of hybrid aerogels.[34] We adopted the Langmuir model and Freundlich model to fit the experimental data (Figure S16 and Table S3). Compared to Langmuir model, Freundlich model is more suitable to describe the uptake process here due to its proper correlation coefficient ($R^2 > 0.97$), indicating a multilayered and heterogeneous I_2 uptake by hybrid aerogels. It is also noted that with an initial I_2 concentration of 1400 mg L^{-1} the hybrid aerogel affords an equilibrium uptake and removal efficiency of 399 mg g^{-1} and 92.7 %, respectively, superior to most of the reported absorbents (Table S4).

3.4. I_2 vapor uptake

Efficiently capturing I_2 vapor represents a practical protocol to alleviate the nuclear radiation leaks.[35] To investigate the volatile I_2 uptake capacity of hybrid aerogels, gravimetric method was used for analysis. Hybrid aerogels were exposed to I_2 vapor under ambient pressure. As temperature has a great influence on the process of guest molecules absorbed in porous materials,[36] we conducted I_2 uptake tests using the hybrid aerogel with 33 wt% COF-LZU1 at various temperatures (Fig. 5**a**). At a low temperature of 15 °C, the hybrid aerogel displays a slow uptake of I_2 vapor, which requires over 250 h to equilibrate. Slightly increasing the temperature to 30 °C accelerates the uptake process, and the equilibrium is achieved within 100 h. Particularly, the I_2 uptake test at 75 °C, which is close to the temperature of actual nuclear-fuel reprocessing, produces a significant uptake capacity of 4.1 g g^{-1} after only 6 h. In fact, the temperature-dominated uptake behavior is partially associated with the variable volatilization rates of I_2 bulks, in which I_2 volatilizes rapidly under high temperatures. The capture of I_2 vapor by hybrid aerogels is mostly attributed to the introduction of COF-LZU1, as demonstrated by the disparate uptake capacity of the pure cellulose aerogel and COF-LZU1 powders (Figure S17). The I_2 uptake capacity of hybrid aerogels with different COF-LZU1 loadings was then measured at 15 °C, with results shown in Fig. 5**b**. It is clear that increasing the loading of COF-LZU1 from 9 to 50 wt% leads to a declined equilibrium uptake capacity. We correlate this result with the blocked accessible pores due to the accumulation of COF-LZU1 particles. In this work, the maximum I_2 adsorption capacity given by the hybrid aerogel is 6.8 g g^{-1}, superior to COF-LZU1 powders and most of the reported studies (Fig. 5**c** and Table S5).

Next, the I_2 storage ability was assessed using the hybrid aerogel with 33 wt% COF-LZU1 under ambient conditions. After exposing to an open environment for 12 days, we can only detect a slight weight loss of < 10 %, showing the relatively stable storage of I_2 in our aerogels (Fig. 5**d**). In addition to the capture and storage of I_2, the release of the captured I_2 from hybrid aerogels is also crucial for practical application.[37] Adsorbed I_2 could be released by soaking these samples in ethanol at room temperature or heating treatment at 125 °C (Fig. 5**e**). Upon soaking in ethanol, a fast and prominent release of the captured I_2 is observed within a short duration of 15 min (Figure S18). Moreover, a soaking time of 120 min generates a high release ratio of up to 79 %. In the case of heating at 125 °C, a relatively slow release behavior is noted and the release percentage reaches 77 % after an extended duration of 400 min. Therefore, ethanol soaking is recognized to be a viable way to recycle I_2 captured in hybrid aerogels.

A diversity of characterizations was applied to probe the mechanism of I_2 uptake by our hybrid aerogels. Physical appearances and SEM observations reveal the structural integrity of aerogels after I_2 uptake (Figure S19, S20). In the FTIR spectra, the characteristic peak of C═N at 1625 cm^{-1} undergoes a red shift after I_2 uptake (Figure S21), implying the interaction between I_2 and C═N bonds. XPS measurements were used to profoundly investigate the chemical state of iodine in hybrid aerogels. As shown in Fig. 5**f**, the characteristic peaks near 619 and 630 eV in the survey spectrum of the hybrid aerogel after I_2 uptake can be assigned to I $3d_{5/2}$ and I $3d_{3/2}$, respectively.[38] In the high-resolution spectrum of I 3d, the two peaks at 617.9 and 629.4 eV are attributed to pentaiodide (I_5^-), while the signals at 619.9 and 631.3 eV are assigned to triiodide (I_3^-) (Fig. 5**g**). Based on the above results, we speculate that the captured iodine exists as iodine molecules and polyiodine anions, which involves the process of physisorption and chemisorption.[39]

3.5. Dynamic I_2 uptake

Dynamic I_2 uptake in a continuous operation holds a huge potential for real-world applications.[40] To confirm the practicality, we shaped the hybrid aerogels into aerogel columns in light of their excellent processability and mechanical stability. For the dynamic removal of I_2 in liquids, I_2 dissolved in *n*-hexane (100 mg L^{-1}) was penetrated through a column composed of 50 mg hybrid aerogel at a flow rate of 0.5 mL min^{-1} (Fig. 6**a**). After passing through the column, the initial purple solution becomes basically colorless, and the UV–vis spectra determine a removal

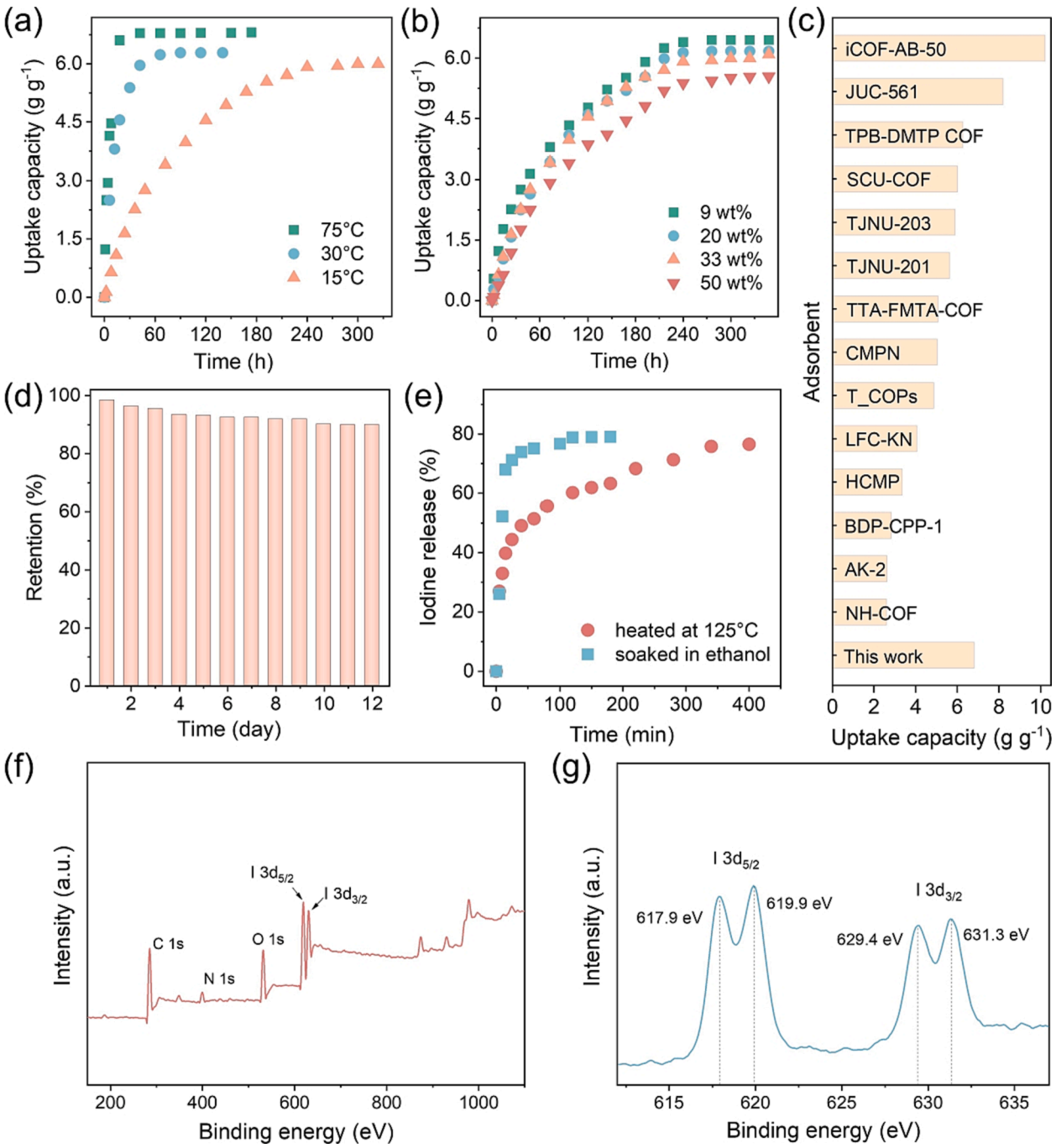

Fig. 5. Evaluation and mechanism of hybrid aerogels for I_2 uptake and recycling. (a) Gravimetric uptake of I_2 vapor by the hybrid aerogel as a function of time under various temperatures. (b) Gravimetric uptake of I_2 vapor by the hybrid aerogels with different COF-LZU1 loadings as a function of time at 15 °C. (c) Comparison of I_2 uptake capacity between our aerogel and other reported adsorbents. (d) I_2 storage ability of hybrid aerogel upon exposure to air at ambient conditions. (e) Release of I_2 from the hybrid aerogel upon heating at 125 °C or soaking in ethanol. (f) Survey XPS spectrum and (g) iodine high-resolution XPS spectrum of the hybrid aerogel after I_2 uptake.

efficiency of 90 % for the first 10 mL solution (Fig. 6**b** and **Figure S22**). The removal efficiency still keeps above 80 % after filtrating 30 mL solution. For the dynamic removal of I_2 vapor, I_2 vapor was carried by flowing N_2 to pass through an aerogel column with a constant flow rate of 40 mL min^{-1} (Fig. 6**c** and **Figure S23a**). After continuously operating for 9 h, the I_2 concentration in ethanol is determined to be a low value of 7.8 μg mL^{-1} (Fig. 6**d** and **Figure S23b**). Therefore, these dynamic tests suggest that our aerogels are highly promising for the continuous removal of radioiodine.

4. Conclusion

In summary, we have developed structurally stable and ultralight COF/cellulose hybrid aerogels through introducing COF-LZU1 particles into the sol–gel process of functionalized CNCs and CMC. In the synthesized hybrid aerogels, cellulose and COF-LZU1 act as the structural skeleton and effective adsorbent, respectively. Hybrid aerogels with the COF-LZU1 loadings in the range of 9–50 wt% are prepared and demonstrate a desired physical stability without structural collapse. The highly porous configuration of hybrid aerogels makes them extremely

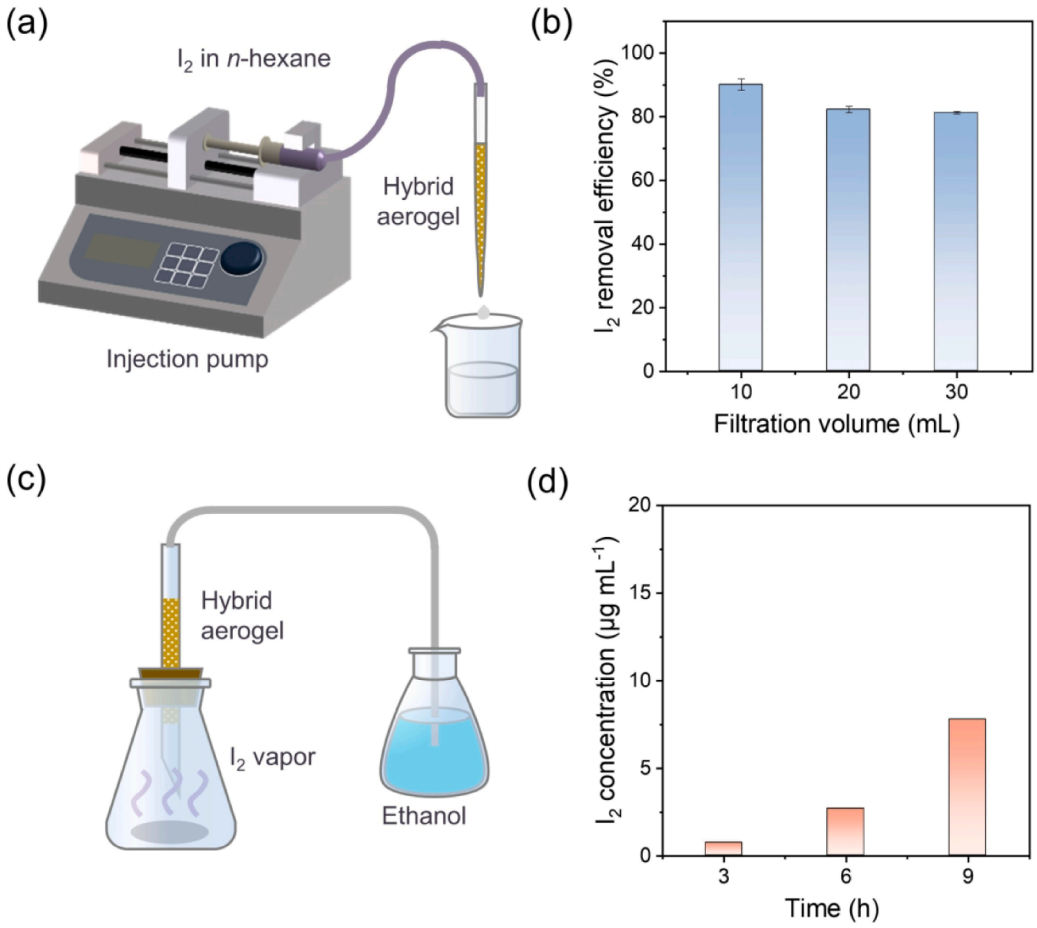

Fig. 6. (a) Schematic diagram showing the continuous capture of I_2 dissolved in *n*-hexane. (b) I_2 removal efficiency of the aerogel column as a function of filtration volume. (c) Schematic diagram showing the continuous capture of I_2 vapor. (d) I_2 concentration in ethanol as a function of operational time.

promising for the absorption of organic solvents. Thanks to the crystalline and microporous COF-LZU1, the prepared hybrid aerogels exhibit an exceptional I_2 capture ability, with an uptake capacity of 399 mg g^{-1} and 6.8 g g^{-1} for dissolved and volatilized I_2, respectively. Moreover, I_2 captured in the aerogel can be easily recycled by soaking in ethanol. We additionally demonstrate the feasibility of removing I_2 solute and vapor in a continuous operation using well-shaped aerogel columns. Therefore, this work paves the way of processing COFs into designated structures and offers insights in designing high-performance adsorbents toward I_2 capture.

CRediT authorship contribution statement

Zhipeng Zhang: Methodology, Investigation, Writing – original draft. **Xiansong Shi:** Writing – review & editing, Funding acquisition. **Xingyuan Wang:** Methodology. **Zhe Zhang:** Methodology. **Yong Wang:** Supervision, Writing – review & editing, Funding acquisition.

Declaration of Competing Interest

The authors declare that they have no known competing financial interests or personal relationships that could have appeared to influence the work reported in this paper.

Data availability

Data will be made available on request.

Acknowledgements

This work was financially supported by the National Natural Science Foundation of China (22008110, 21921006).

Appendix A. Supplementary data

Supplementary data to this article can be found online at https://doi.org/10.1016/j.seppur.2023.123108.

References

[1] P.A. Kharecha, J.E. Hansen, Prevented mortality and greenhouse gas emissions from historical and projected nuclear power, Environ. Sci. Technol. 47 (9) (2013) 4889–4895.
[2] J. Dai, S. Li, J. Bi, Z. Ma, The health risk-benefit feasibility of nuclear power development, J. Clean. Prod. 224 (2019) 198–206.
[3] N. Yoshida, J. Kanda, Tracking the fukushima radionuclides, Science 336 (6085) (2012) 1115–1116.
[4] T. Geng, C. Zhang, M. Liu, C. Hu, G. Chen, Preparation of biimidazole-based porous organic polymers for ultrahigh iodine capture and formation of liquid complexes with iodide/polyiodide ions, J. Mater. Chem. A 8 (5) (2020) 2820–2826.
[5] F.C. Kupper, M.C. Feiters, B. Olofsson, T. Kaiho, S. Yanagida, M.B. Zimmermann, L. J. Carpenter, G.W. Luther, Z. Lu, M. Jonsson, L. Kloo, Commemorating two centuries of iodine research: an interdisciplinary overview of current research, Angew. Chem. Int. Ed. 50 (49) (2011) 11598–11620.
[6] A. Saiz-Lopez, J.M. Plane, A.R. Baker, L.J. Carpenter, R. von Glasow, J.C. Martin, G. McFiggans, R.W. Saunders, Atmospheric chemistry of iodine, Chem. Rev. 112 (3) (2012) 1773–1804.
[7] K. Geng, T. He, R. Liu, S. Dalapati, K.T. Tan, Z. Li, S. Tao, Y. Gong, Q. Jiang, D. Jiang, Covalent organic frameworks: design, synthesis, and functions, Chem. Rev. 120 (16) (2020) 8814–8933.

[8] C.S. Diercks, O.M. Yaghi, The atom, the molecule, and the covalent organic framework, Science 355 (6328) (2017) eaal1585.
[9] C. Yin, Z. Li, D. Zhao, J. Yang, Y. Zhang, Y. Du, Y. Wang, Azo-branched covalent organic framework thin films as active separators for superior sodium−sulfur batteries, ACS Nano 16 (2022) 14178–14187.
[10] C. Yin, Z. Zhang, Z. Si, X. Shi, Y. Wang, Smart covalent organic frameworks with intrapore azobenzene groups for light-gated ion transport, Chem. Mater. 34 (2022) 9212–9220.
[11] X. Shi, Z. Zhang, C. Yin, X. Zhang, J. Long, Z. Zhang, Y. Wang, Design of three-dimensional covalent organic framework membranes for fast and robust organic solvent nanofiltration, Angew. Chem. Int. Ed. 61 (36) (2022) e202207559.
[12] Z. Xu, Q. Zhang, P. Lin, Y. Gao, Y. Wen, K. Li, L. Li, Oxygen-rich microporous carbons with exceptionally high adsorption of iodine, Mater. Chem. Phys. 285 (2022), 126193.
[13] A. Al-Mamoori, M. Alsalbokh, S. Lawson, A.A. Rownaghi, F. Rezaei, Development of bismuth-mordenite adsorbents for iodine capture from off-gas streams, Chem. Eng. J. 391 (2020), 123583.
[14] X. Hu, H. Wang, C.F.J. Faul, J. Wen, Y. Wei, M. Zhu, Y. Liao, A crosslinking alkylation strategy to construct nitrogen-enriched tetraphenylmethane-based porous organic polymers as efficient carbon dioxide and iodine adsorbents, Chem. Eng. J. 382 (2020), 122998.
[15] B. Valizadeh, T.N. Nguyen, B. Smit, K.C. Stylianou, Porous metal-organic framework@polymer beads for iodine capture and recovery using a gas-sparged column, Adv. Funct. Mater. 28 (30) (2018) 1801596.
[16] Z.J. Yin, S.Q. Xu, T.G. Zhan, Q.Y. Qi, Z.Q. Wu, X. Zhao, Ultrahigh volatile iodine uptake by hollow microspheres formed from a heteropore covalent organic framework, Chem. Commun. 53 (53) (2017) 7266–7269.
[17] P. Wang, Q. Xu, Z. Li, W. Jiang, Q. Jiang, D. Jiang, Exceptional iodine capture in 2D covalent organic frameworks, Adv. Mater. 30 (2018) e1801991.
[18] M.E. Carrington, N. Rampal, D.G. Madden, D. O'Nolan, N.P.M. Casati, G. Divitini, J.Á. Martín-Illán, M. Tricarico, R. Cepitis, C. Çamur, T. Curtin, J. Silvestre-Albero, J.-C. Tan, F. Zamora, S. Taraskin, K.W. Chapman, D. Fairen-Jimenez, Sol-gel processing of a covalent organic framework for the generation of hierarchically porous monolithic adsorbents, Chem 8 (2022) 1–17.
[19] S. Kandambeth, K. Dey, R. Banerjee, Covalent organic frameworks: chemistry beyond the structure, J. Am. Chem. Soc. 141 (5) (2019) 1807–1822.
[20] D. Zhu, Y. Zhu, Q. Yan, M. Barnes, F. Liu, P. Yu, C.-P. Tseng, N. Tjahjono, P.-C. Huang, M.M. Rahman, E. Egap, P.M. Ajayan, R. Verduzco, Pure crystalline covalent organic framework aerogels, Chem. Mater. 33 (11) (2021) 4216–4224.
[21] J.A. Martin-Illan, D. Rodriguez-San-Miguel, O. Castillo, G. Beobide, J. Perez-Carvajal, I. Imaz, D. Maspoch, F. Zamora, Macroscopic ultralight aerogel monoliths of imine-based covalent organic frameworks, Angew. Chem. Int. Ed. 60 (25) (2021) 13969–13977.
[22] Z. He, F. Wu, S. Guan, L. Liu, J. Li, Y. Huang, Polyamide amine/aramid nanofiber composite aerogels as an ultra-high capacity adsorbent for Congo red removal, J. Mater. Chem. A 9 (22) (2021) 13320–13331.
[23] Y. Sun, Y. Chu, W. Wu, H. Xiao, Nanocellulose-based lightweight porous materials: A review, Carbohydr. Polym. 255 (2021), 117489.
[24] Y. Wu, Y. Li, T. Zhao, X. Wang, V.I. Isaeva, L.M. Kustov, J. Yao, J. Gao, Bimetal-organic framework-derived nanotube@cellulose aerogels for peroxymonosulfate (PMS) activation, Carbohyd. Polym. 296 (2022), 119969.
[25] F. Li, L.-G. Ding, B.-J. Yao, N. Huang, J.-T. Li, Q.-J. Fu, Y.-B. Dong, Pd loaded and covalent-organic framework involved chitosan aerogels and their application for continuous flow-through aqueous CB decontamination, J. Mater. Chem. A 6 (24) (2018) 11140–11146.
[26] M.M. Hamedi, A. Hajian, A.B. Fall, K. Hakansson, M. Salajkova, F. Lundell, L. Wagberg, L.A. Berglund, Highly conducting, strong nanocomposites based on nanocellulose-assisted aqueous dispersions of single-wall carbon nanotubes, ACS Nano 8 (3) (2014) 2467–2476.
[27] H. Yang, L. Yang, H. Wang, Z. Xu, Y. Zhao, Y. Luo, N. Nasir, Y. Song, H. Wu, F. Pan, Z. Jiang, Covalent organic framework membranes through a mixed-dimensional assembly for molecular separations, Nat. Commun. 10 (1) (2019) 2101.
[28] C. Zhu, S. Pang, Z. Chen, L. Bi, S. Wang, C. Liang, C. Qin, Synthesis of covalent organic frameworks (COFs)-nanocellulose composite and its thermal degradation studied by TGA/FTIR, Polymers 14 (15) (2022) 3158.
[29] S.Y. Ding, J. Gao, Q. Wang, Y. Zhang, W.G. Song, C.Y. Su, W. Wang, Construction of covalent organic framework for catalysis: Pd/COF-LZU1 in Suzuki-Miyaura coupling reaction, J. Am. Chem. Soc. 133 (49) (2011) 19816–19822.
[30] H. Fan, A. Mundstock, A. Feldhoff, A. Knebel, J. Gu, H. Meng, J. Caro, Covalent organic framework-covalent organic framework bilayer membranes for highly selective gas separation, J. Am. Chem. Soc. 140 (32) (2018) 10094–10098.
[31] X. Yang, E.D. Cranston, Chemically cross-linked cellulose nanocrystal aerogels with shape recovery and superabsorbent properties, Chem. Mater. 26 (20) (2014) 6016–6025.
[32] H. Zhu, X. Yang, E.D. Cranston, S. Zhu, Flexible and porous nanocellulose aerogels with high loadings of metal-organic-framework particles for separations applications, Adv. Mater. 28 (35) (2016) 7652–7657.
[33] X. Li, Y. Wang, Y. Mu, J. Gao, L. Zeng, Oriented construction of efficient intrinsic proton transport pathways in MOF-808, J. Mater. Chem. A 10 (2022) 18592–18597.
[34] Y.G. Zhu, Y.Z. Huang, Y. Hu, Y.X. Liu, Iodine uptake by spinach (Spinacia oleracea L.) plants grown in solution culture: effects of iodine species and solution concentrations, Environ. Int. 29 (1) (2003) 33–37.
[35] W. Xie, D. Cui, S.-R. Zhang, Y.-H. Xu, D.-L. Jiang, Iodine capture in porous organic polymers and metal-organic frameworks materials, Mater. Horiz. 6 (8) (2019) 1571–1595.
[36] R. Krishna, Describing the diffusion of guest molecules inside porous structures, J. Phys. Chem. C 113 (46) (2009) 19756–19781.
[37] B. Akram, Q. Lu, X. Wang, Polyoxometalate-zirconia coassembled microdumbbells for efficient capture of iodine, ACS Mater. Lett. 2 (5) (2020) 461–465.
[38] X. Li, Z. Jia, J. Zhang, Y. Zou, B. Jiang, Y. Zhang, K. Shu, N. Liu, Y. Li, L. Ma, Moderate and universal synthesis of undoped covalent organic framework aerogels for enhanced iodine uptake, Chem. Mater. 34 (24) (2022) 11062–11071.
[39] J. Chang, H. Li, J. Zhao, X. Guan, C. Li, G. Yu, V. Valtchev, Y. Yan, S. Qiu, Q. Fang, Tetrathiafulvalene-based covalent organic frameworks for ultrahigh iodine capture, Chem. Sci. 12 (24) (2021) 8452–8457.
[40] L. He, L. Chen, X. Dong, S. Zhang, M. Zhang, X. Dai, X. Liu, P. Lin, K. Li, C. Chen, T. Pan, F. Ma, J. Chen, M. Yuan, Y. Zhang, L. Chen, R. Zhou, Y. Han, Z. Chai, S. Wang, A nitrogen-rich covalent organic framework for simultaneous dynamic capture of iodine and methyl iodide, Chem 7 (3) (2021) 699–714.